

Amorphous infinite coordination polymers  
and their synthesis from a novel set of  
organic ligands

By

Adam Kewley

2010

A Project Report presented in part  
consideration for the degree of

*MSc Nanoscience*

In dedication to my family who have supported me throughout the many trials during my four years at the University of Nottingham.

## Summary

This report shall be studying the synthesis of a novel ligand and its use in creating an amorphous infinite coordination polymer (ICP) with multiple metal species. To increase the comprehensiveness of this study, ICPs were also made with a similar, but established, ligand originally developed by the research group. Much of this report is focused on the characterization of these exciting compounds with the hope of uncovering a useful functionality.

The potential of ICPs is briefly discussed and a discussion about previous works in this field follows this. Many well-established pioneers in this field are identified and, more importantly, the imaginative ways in which they have developed this exciting research field are mentioned. Following this, the synthesis of our ligand systems is comprehensively described. Characterization of the ligand and coordination systems produces some interesting results regarding the structure and properties of these materials. And while the study is concluded to produce some interesting findings the outlook for this particular class of particles is concluded to be even more promising.

## Contents

Summary .....	3
Introduction .....	5
Literature Review .....	6
Experimental .....	11
Ligand syntheses.....	11
ICP syntheses .....	14
Results & Discussion.....	17
The ligands.....	17
Analysis of the novel benzene centred ligands (L1&L3).....	17
Analysis of the naphthalene centred ligand (L2) .....	21
ICPs.....	22
Conclusion.....	35
References .....	36
Appendix.....	37

# Introduction

In recent years, metal-organic frameworks (MOFs) have received a large amount of scientific interest. These are frameworks consisting of metal ions or clusters that coordinate with rigid organic molecules (linkers) to form one-, two-, or three-dimensional structures that can be porous<sup>1-4</sup>. This interest arises from the wide variety of possible applications of these frameworks: catalysis, gas storage, and molecular recognition to name a few. The two components of a MOF, the metal and linker, each have an effect on the types of pores that make up the structure; for example, a metal's coordination preference influences the size and shape of the pores. Likewise, the length, chemistry, and rigidity of the linkers have an effect not only on the size and shape of the pore, but the possible compounds that may occupy them. This flexibility in design is attractive and allows the researcher to postulate a needs-based design. That is to say, provided they form a structure predictably, the frameworks could be chemically tailored to meet a specification based on knowledge about the metals and linkers used.

However, there is one major limitation to MOFs. They are macroscopic and have very limited solution-based behaviour<sup>1</sup>. This means they must, for the most part, be handled as solids. These practicalities can put a limitation on the applicability of MOFs in certain areas of industry such as medicine.

One alternative approach to creating the ordered, porous, and functional structure of MOFs while still maintaining a reasonable degree of solution-based behaviour is to create a polymerised coordination structure. Here, instead of discrete motifs that come together to create the overall solid, the framework is created by the coordination polymerisation of metal ions connected through multidentate ligands. The resulting materials, so called infinite coordination polymers (ICP), have been reported show remarkable stability and may be dispersed in a range of solvents<sup>2,4-9</sup>. Many syntheses involve fast precipitation of the ICP to create discrete nano- and micro-scale particles which can increase the effective surface area of the material. This fast precipitation can also mechanically trap other functional species within the material, such as magnetic nanoparticles, and organic dyes allowing for even greater control over the functional properties of the resulting particles<sup>1,2</sup>.

Here, the synthesis of a novel linker and its use with different metal centres shall be explored with the hope of creating ICP particles. Several synthetic challenges are presented by such syntheses; for example, the structural characterization of the ICP itself. Such challenges shall be approached as systematically as possible for this novel class of particles. The target ligand system for this study is based on initial studies

by V. J. Richards with one ligand being a direct repeat of an experimental procedure. These species, by contrast to other MOF linkers, contain a reasonably flexible backbone which may introduce a new level of amorphicity into the resultant particles. Because of this, characterization and discussion of the findings is a central part of this study and as such are an accordingly large presence in this report.

Nevertheless, the potential of these ligands and, more importantly, the ICPs they may go on to fabricate is tremendous when considering the large array of potential guests, metals, and structural analogues that are possible.

## Literature Review

To gain an initial insight into the challenges and opportunities encountered when dealing with ICPs two reviews written by S. L. James and C. A. Mirkin et. al. in MOFs and ICPs respectively were found to be an excellent primary source of information<sup>3,4</sup>.

Synthesis of ICPs generally appears to involve the reaction of a multidentate ligand with a metal salt to create a coordination polymer. While this was mentioned in the introduction, the exact method for producing discrete particles was not discussed. It appears that there is a choice of three methods: (a) solvothermal synthesis (analogous to hydrothermal synthesis), (b) microemulsion based techniques, and (c) formation and precipitation of the particles triggered by introduction of a solvent into the solution of the ligands and metal cations (i.e. crash the particles out of solution). Of these (c) is by far the most commonly used method<sup>4</sup>.

Solvent-induced precipitation of the particles arrests further polymerisation of the compounds allowing for a degree of control over their final size. For this, metal cation and organic ligand are dissolved in a solvent, in which they and the resulting ICPs are highly soluble. A second solvent is then introduced into the system to induce precipitation of the ICPs. This process of precipitation assumes that the ICP, ligand, and metal cooperate with a particular solvent system which may not be the case for this study. The 'crashing out' of the ICP means that it will generally have an amorphous or crystalline structure distinct from the thermodynamically preferred (MOF) solid-state structure. This distinct structure can have significantly different properties from their MOF which needs to be considered when working with the crystal structures of ICPs.

Mirkin et. al. have also proposed a mechanism for growth based on time-resolved scanning electron microscopy (SEM) which may provide a valuable insight into the observations made for the systems this study focuses on<sup>4,7</sup>. It suggests a mechanism of initial seed generation during the early stages of the reaction due to the high

concentrations of metal and ligand present. This is then followed by aggregation of these small particles to form larger initial particles which, because there are unreacted sites at their surface, then go on to fuse to form larger particles. The final stages of growth involve the annealing of the particles in the remaining reaction mixture (which now has a low reagent concentration) into the final spherical ICP particles (Figure 1).

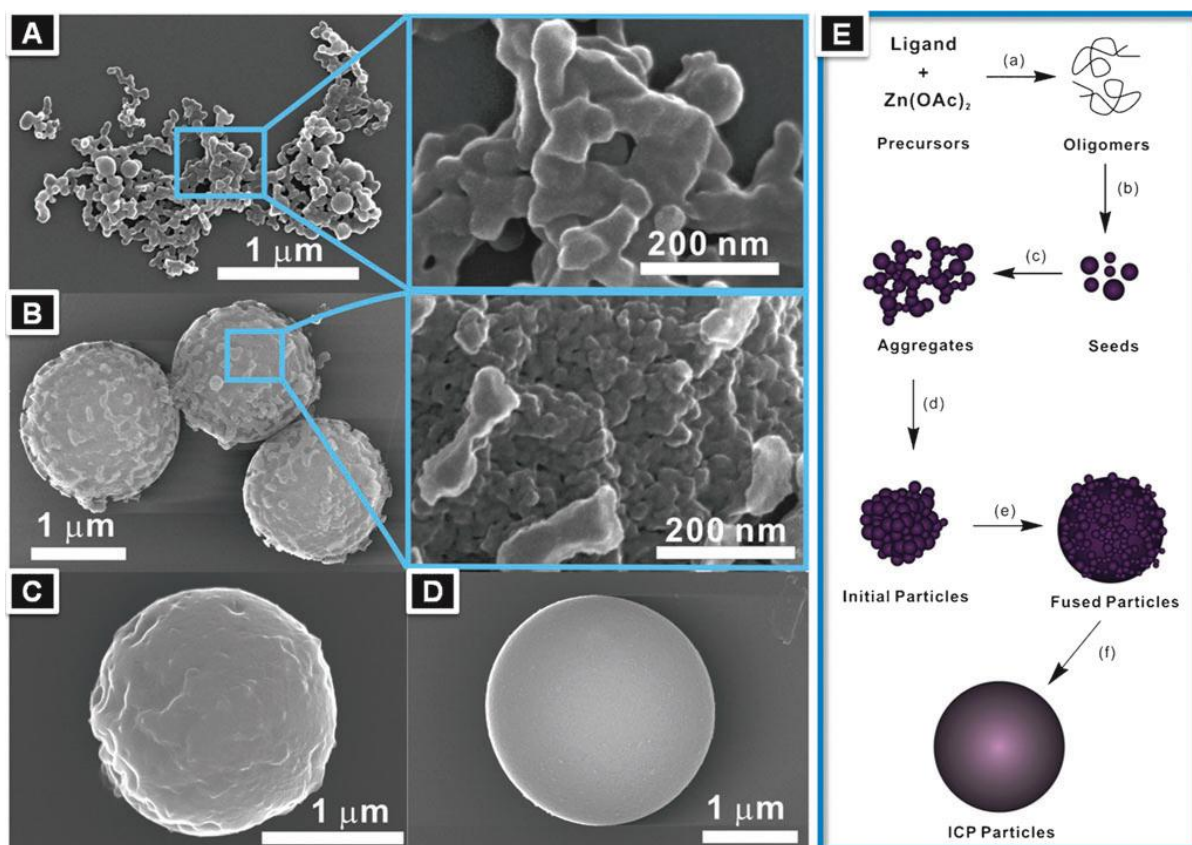


**Figure 1** A representative mechanism for the formation of spherical ICP particles (based on a Troger's base 7-based synthesis). (A)-(D) Time resolved SEM study and (C) the proposed working mechanism for ICP particle formation. Reprinted from a reference source<sup>4,7</sup>.

Other works by Jung and Oh have observed the formation of nanocubes based on the same mechanism from nanowire seeds<sup>8</sup>. As Mirkin et. al. report, one of the limitations in the field of ICPs is the lack of information on the growth process which can lead to some generalities when explaining the observed particles of a reaction<sup>4</sup>.

One interesting point that was made in the introduction about these particles is their ability to have highly tailored properties due to the wide choice of ligands and metals. The introduction of magnetic properties by a valence tautomeric system has been reported<sup>2,5</sup>. Magnetism is an especially exciting area of interest for these solution stable materials because of its wide reaching potential in the field of MRI contrast agents. ICPs composed of lanthanides have exhibited promise for these applications<sup>4</sup>. Optical properties are also another area of interest for these materials. Mirkin et. al. report a

system with modifiable optical properties. In this system the colour of the ICP can be modified by changing the solvent-guest which coordinates to the metal centre, allowing for a colour change based on the solvent present (Figure 2). These types of effects, although not a specific target for this study, shall be kept in mind if any similarities are found.

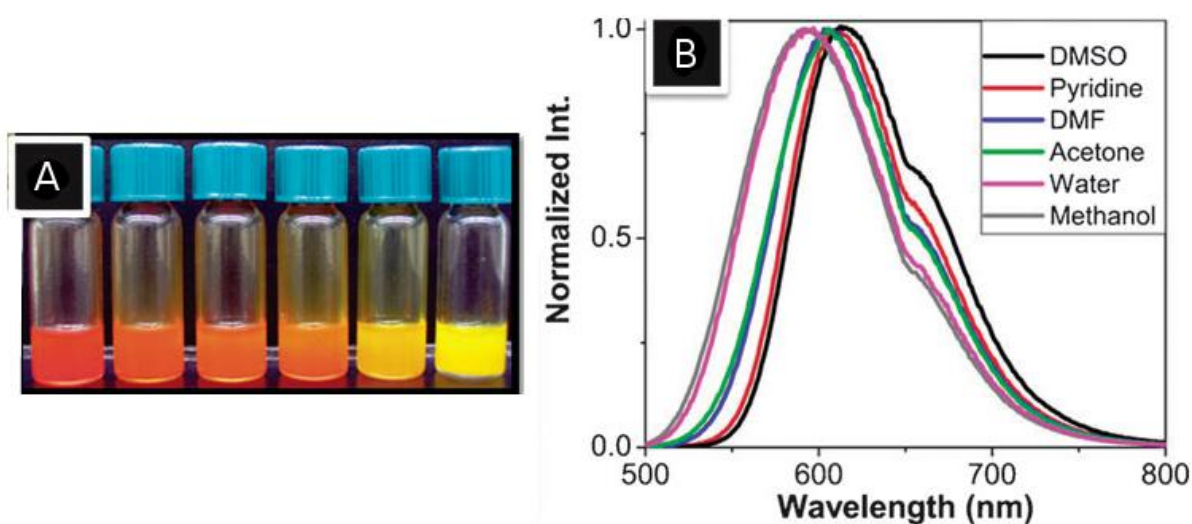


**Figure 2** The range of optical properties found for bis-metallo-tridentate Schiff base (BMSB) in a range of solvents. (A) Particles in different solvents observed with the naked eye (from left to right: DMSO to methanol, as in the order of (B)), and (B) UV-vis spectroscopy of the particles. Modified from a reference source<sup>9</sup>.

While the chemical functionality of the ligand and metal are of great interest when considering the applications of ICPs, another interesting modification that may be made is to encapsulate other functional compounds within them (Figure 3). Maspoch et. al. report the fast precipitation of ICPs made from  $Zn^{II}$  metal ions and 1,4-bis(imidazole-1-ylmethyl)benzene (bix) can mechanically trap the desired functional species present in the reaction mixture<sup>2</sup>. The methodology involved mixing the metal ions, ligand, and 10nm diameter magnetic iron oxide nanoparticles together with vigorous stirring at room temperature followed by precipitation by solvent introduction. The resulting particles had the properties expected of Zn(bix) spheres but additionally had the magnetic properties of the iron oxide nanoparticles creating a sort of 'hybrid' particle.

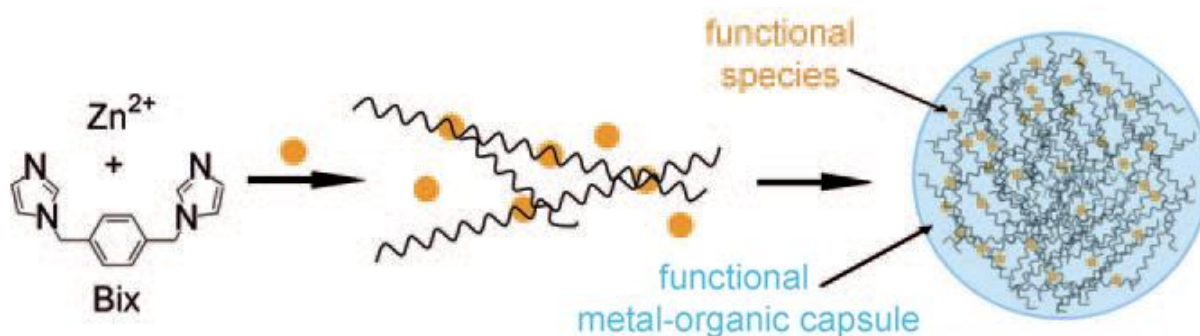


**Figure 3 Schematic illustration of the simultaneous formation and encapsulation of functional species in metal-organic Zn (bix) micro- and nano-spheres. Reprinted from a reference source<sup>1</sup>.**

The field of encapsulation opens up a whole new avenue of interest for ICPs. There is already extensive research in the field of single-component nanoparticles (made by salt reduction and the like) that provide many sources of possible particles for encapsulation. Combining the useful properties of nanoparticles with the properties of ICPs to form stable multifunctional compounds introduces an extensive amount of possibilities for the imaginative researcher in an already expansive field.

There are some problems in the synthesis of ICPs however. The first problem, as described by S. L. James, is predicting the network geometry<sup>3</sup>. In principle, it is only necessary to react a potentially bridging ligand with a metal ion which has more than one vacant or labile site. The most detailed structural information, like in any novel synthetic venture, will be gained from single crystal X-ray crystallography. Without knowing the crystal structure it is hard to interpret the observed properties of these materials. This biases research in ICPs towards systems that can produce well-ordered, as opposed to highly amorphous, structures. To achieve this order, two primary considerations must be made: the lability of the metal-ligand bond, and the flexibility of the ligand.

The lability (i.e. the reversibility of) the metal-ligand bond is important because a reversible reaction can allow for rearrangement of the structure into the most thermodynamically preferable arrangement (i.e. a geometrically sound crystalline structure). However, a problem with highly labile metal ions is that they do not impose as much of a preference for a given geometry as compared with other ions which can lead to a lack of predictability in the structure.

The flexibility of the ligand also plays a key role when considering the predictability of a ICPs structure. The orientational freedom can be reduced by using rigid backbones. The most commonly used rigid backbones being some form of planar aromatic compound such as naphthalene or 2,2-bipyridine. Some of these may have a slight amount of

rotational freedom but, most importantly, such rotation does not affect the mutual orientation of the donors.

The target ligands for this study are shown in Figure 4. L2 is part of an ongoing study by N. Champness et. al. as a possible ICP ligand candidate; therefore, synthesis of this ligand shall be a direct repeat of previous works. L1 and L3 are novel benzene centred analogues of L2. What is immediately apparent, taking patterns in the literature into account, is the apparent flexibility of the backbone. This could potentially lead to highly amorphous compounds. Likewise, the tetradentate nature of L1 introduces a degree of unpredictability when working with these compounds. However, this flexibility may increase the range of possible particle sizes for encapsulation. Undoubtedly, the flexibility of these ligands shall hopefully provide an insight into the breadth of possible ligands that may be used in ICPs.

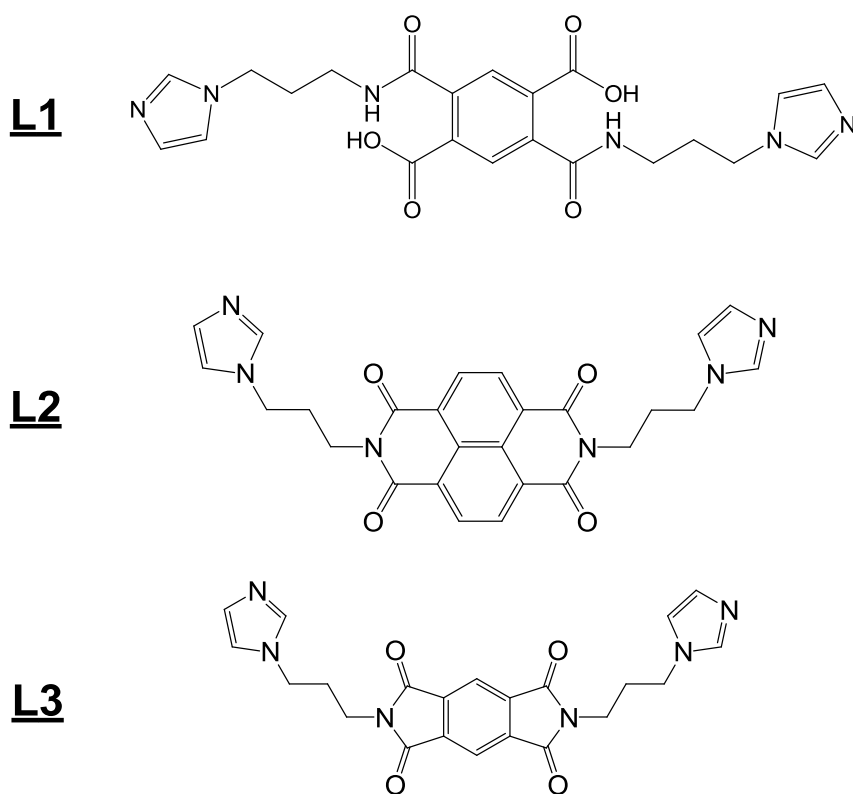
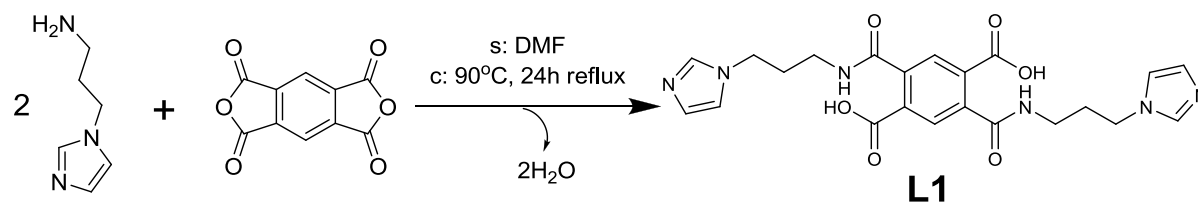


**Figure 4** The target ligands for this study. Top: 2,5-bis(3-(1H-imidazol-1-yl)propylcarbamoyl) terephthalic acid, middle: 2,7-bis(3-(1H-imidazol-1-yl)propyl) benzo[lmn][3,8]phenanthroline-1,3,6,8(2H,7H)-tetraone, bottom: 2,6-bis(3-(1H-imidazol-1-yl)propyl)pyrrolo[3,4-f]isoindole-1,3,5,7(2H,6H)-tetraone. Each shall be referred to as L1, L2, and L3 respectively for the rest of the report due to their cumbersome names.

# Experimental

## Ligand syntheses

1-(3-Aminopropyl) imidazole (98%), benzene-1,2,4,5-tetracarboxylic dianhydride (97%), and 1,4,5,8-naphthalenetetracarboxylic dianhydride were purchased from Sigma-Aldrich (St. Lewis, MO).



**Scheme 1 Synthetic route to 2,5-bis(3-(1H-imidazol-1-yl)propylcarbamoyl)terephthalic acid (L1).**

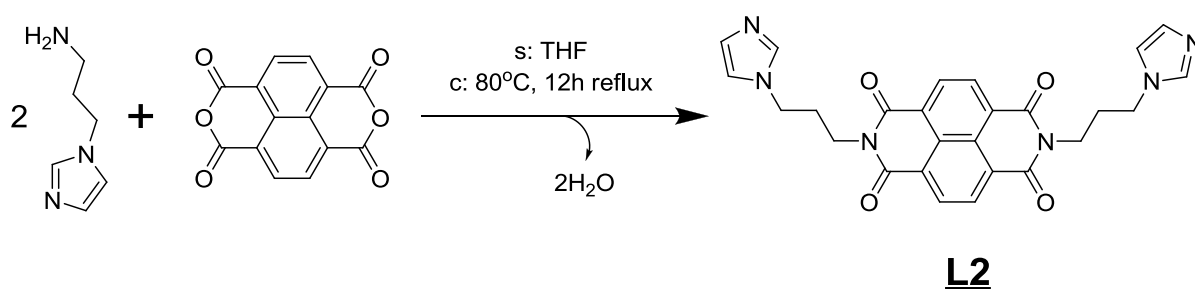
The synthesis of 2-(2-(1H-imidazol-1-yl)ethylcarbamoyl)-5-(3-(1H-imidazol-1-yl)propylcarbamoyl)terephthalic acid (L1) is outlined in Scheme 1. 1-(3-Aminopropyl) imidazole (1.3mL, 10mmol) was added to a solution of Benzene-1,2,4,5-tetracarboxylic dianhydride (1.08g, 4.95mmol) dissolved in dimethylformamide (DMF, 10mL), immediate formation of a white polymer-like solid was observed. The reaction mixture was refluxed for 24h at 90°C and cooled to room temperature resulting in a yellow tinted suspension. The precipitate was collected by suction filtration and washed briefly with DMF to isolate a white solid. Purification was performed by crystallization from a DMF/ethanol mixture (3/1 by volume) followed by drying under vacuum.

Characterization was assessed with numerous techniques: proton nuclear magnetic resonance (<sup>1</sup>H NMR), carbon-13 NMR (<sup>13</sup>C NMR), Fourier transform infrared spectroscopy (FTIR), elemental analysis, single-crystal X-Ray diffraction, and matrix assisted laser desorption/ionization-time of flight mass spectrometry (MALDI-TOF). <sup>1</sup>H NMR (400MHz DMSO-d<sub>6</sub>) δ 8.50 (s, 2 H), 8.48 (s, 2 H), 7.55 (s, 2 H), 7.36 (s, 2 H), 4.20 (t, J = 7.2 Hz, 4 H), 3.65 (t, J = 6.7 Hz, 4 H), 2.17 (q, J = 7.0 Hz, 4 H) (appendix A15). <sup>13</sup>C-DEPT NMR (101 MHz DMSO-d<sub>6</sub>) δ 29.00 (CH<sub>2</sub>), 35.92 (CH<sub>2</sub>), 46.25 (CH<sub>2</sub>), 120.26 (CH), 121.61 (CH), 126.70 (CH), 135.13 (CH), 136.03 (C), 138.39 (C), 171.86 (C), 174.18 (C) (appendix A16&17). FTIR showed numerous peaks for later analysis (appendix A1). Elemental analysis: C: 55.09, H: 4.42, N: 15.78; expected: C: 56.4, H: 5.16, N: 17.9. Single crystal-crystal X-Ray diffraction carried out on crystals unintentionally made from L1 MOF crystallizations (sec. MOF syntheses) shown, in addition to other information, the ring opened structure. MALDI-TOF contained many peaks but did not include the

expected peak with mass 468.18Da (appendix A13). Solubility tests were also performed to determine an ideal solvent for later syntheses:

**Table 1 Solubility of L1**

L1 solubility	
Soluble	Insoluble
Water	Methanol, acetonitrile, tetrahydrofuran, chloroform, isopropyl alcohol, dimethylformamide, acetone, dimethyl sulfoxide, ethyl acetate, ethanol



**Scheme 2 Synthetic route to 2,7-bis(3-(1H-imidazol-1-yl)propyl)benzo[Imn][3,8]phenanthroline-1,3,6,8(2H,7H)-tetraone (L2)**

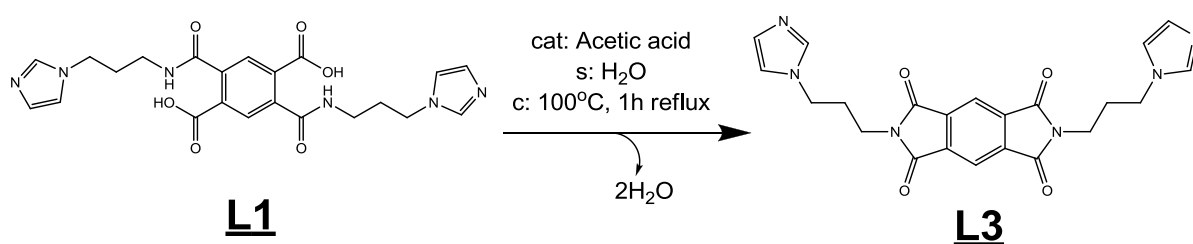
The synthesis of 2,7-bis(3-(1H-imidazol-1-yl)propyl)benzo[Imn][3,8]phenanthroline-1,3,6,8(2H,7H)-tetraone (L2) is outlined in Scheme 2. 1-(3-Aminopropyl) imidazole (5.5mL, 46mmol) was added to a solution of 1,4,5,8-naphthalenetetracarboxylic dianhydride (4g, 15mmol) in tetrahydrofuran (THF, 70mL). The reaction mixture was refluxed for 12h at 80°C and cooled to room temperature resulting in a brown liquid with suspended yellow-tinted solids. The precipitate was collected by suction filtration and washed briefly with DMF. Purification was performed based on a reference procedure<sup>10</sup>. The precipitate was recrystallized by dissolving it in a boiling chloroform/ethanol (1/1 by volume) mixture and removing impurities by suction filtration. Upon cooling, precipitated yellow solid was isolated by suction filtration through a fine fritted funnel and dried under vacuum.

Characterization was performed with several techniques: <sup>1</sup>H NMR, FTIR, elemental analysis, and electrospray mass spectrometry (ES-MS). <sup>1</sup>H NMR (400MHz CDCl<sub>3</sub>) δ 8.78 (s, 4 H), 7.55 (s, 2 H), 7.07 - 6.96 (m, 4 H), 4.30 (t, J = 7.0 Hz, 4 H), 4.14 (t, J = 7.0 Hz, 4 H), 2.33 (q, J = 7.0 Hz, 4 H) (appendix A18). FTIR shown numerous peaks for later analysis (appendix A6). Elemental analysis: C: 64.82, H: 4.48, N: 17.36; expected: C: 64.72, H: 4.6, N: 17.41. ES-MS had shown the expected molecular ion peak with

mass 482.17Da (appendix A14). Solubility tests were also performed to determine an ideal solvent for later syntheses:

**Table 2 Solubility of L2**

L2 solubility	
Soluble	Insoluble
Chloroform, acetonitrile, dichloromethane, ethanol (+Δ, precipitates upon cooling), butanol (+Δ, precipitates upon cooling), ethanol/chloroform (1/1 by volume)	Water, ethyl acetate, acetone, hexane, isopropanol, diethyl ether



**Scheme 3 Synthetic route to 2,6-bis(3-(1H-imidazol-1-yl)propyl)pyrrolo[3,4-f]isoindole-1,3,5,7(2H,6H)-tetraone (L3)**

The synthesis of 2,6-bis(3-(1H-imidazol-1-yl)propyl)pyrrolo[3,4-f]isoindole-1,3,5,7(2H,6H)-tetraone (L3) is outlined in Scheme 3. L1 in an acetic acid/ water (1/1 by volume) mixture was refluxed for 3h at 100°C. The reaction mixture was rotary evaporated to yield an oily substance which precipitated over four days in air. The resulting solid was washed with copious cold water to remove trace acetic acid and starting material. Purification was performed by recrystallizing the solid from boiling water and collecting the resulting acicular (needle-like) crystals by suction filtration followed by vacuum drying.

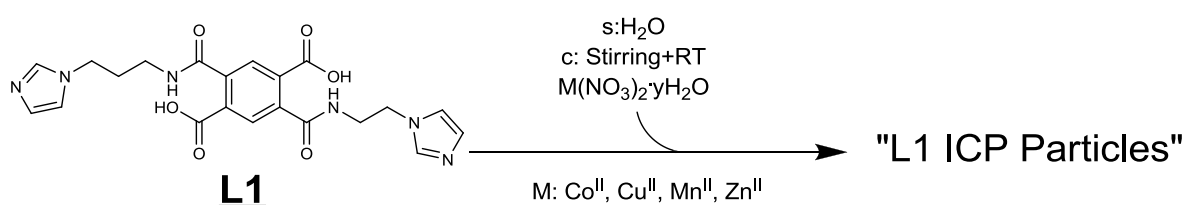
Characterization was performed with several techniques:  $^1\text{H}$  NMR,  $^{13}\text{C}$  DEPT NMR, FTIR, and elemental analysis.  $^1\text{H}$  NMR (400MHz DMSO-d<sub>6</sub>)  $\delta$  8.50 (s, 2 H), 8.48 (s, 2 H), 7.55 (s, 2 H), 7.36 (s, 2 H), 4.20 (t, J = 7.2 Hz, 4 H), 3.65 (t, J = 6.6 Hz, 4 H), 2.17 (q, J = 7.0 Hz, 4 H) (appendix A19).  $^{13}\text{C}$  NMR (101 MHz DMSO-d<sub>6</sub>)  $\delta$  29.26 (CH<sub>2</sub>), 35.62 (CH<sub>2</sub>), 45.71 (CH<sub>2</sub>), 121.46 (CH), 123.78 (CH), 134.55 (CH), 135.79 (CH), 137.46 (C), 166.86 (C) (appendix A20&21). FTIR shown numerous peaks for later analysis (appendix A12). Elemental analysis: C: 55.56 H: 4.01 N: 10.31; expected, C: 61.10, H: 4.66, N: 19.43. Solubility tests were also performed to determine an ideal solvent for later syntheses:

**Table 3 Solubility of L3**

L3 solubility	
Soluble	Insoluble
Water (+Δ, precipitates upon cooling)	Diethyl ether, ethanol, dichloromethane, acetonitrile, benzene

## ICP syntheses

Copper(II) nitrate hemi(pentahydrate) (>98%), cobalt(II) nitrate hexahydrate (>98%), manganese(II) nitrate hydrate (>98%), and zinc nitrate hexahydrate (>98%) were purchased from Sigma-Aldrich (St. Lewis, MO). Ligands were prepared as explained previously.



### Scheme 4 Syntheses of L1 ICP particles from ligand precursor and metal nitrate salts

**Table 4 Quantities of metal salt reagents for L1 ICP syntheses and the resulting post-reaction precipitate colour**

M	Quantity	Precipitate colour
Co <sup>II</sup>	125mg, 0.43mmol	Pink
Cu <sup>II</sup>	86.7mg, 0.37mmol	Deep blue
Mn <sup>II</sup>	76mg, 0.43mmol	White
Zn <sup>II</sup>	128mg, 0.43mmol	White

The syntheses of the L1 ICP particles are outlined in Scheme 5 with reagent quantities shown in Table 4. In each case, a solution of L1 (200mg, 0.43mmol) in a minimum amount of water was added to a magnetically stirred solution of metal salt (Table 1) in a minimum amount of water at room temperature and left to stir for approximately 15min\*. The resulting suspension was then separated by centrifugation and decantation followed by drying under vacuum to isolate a light particulate solid.

\* With the exception of manganese nitrate which required 4 days of stirring before precipitate formation.

† Noting that the rate of precipitation for L2 ICP syntheses was much higher than that of

Characterization of the resulting solids were performed with several techniques: atomic force microscopy (AFM), FTIR, and elemental analysis. AFM and FTIR both yielded results for analysis in the discussion section (appendix A2-5). Elemental analysis results are shown in Table 5 for each metal respectively.

**Table 5 The elemental compositions of L1 ICP syntheses**

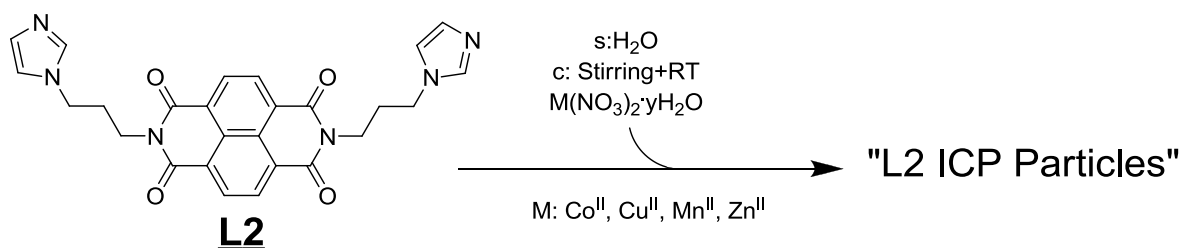
Metal	Elemental composition					
	Found			Expected (1equiv metal)		
	C	H	N	C	H	N
Co <sup>II</sup>	53.63	3.86	16.83	50.10	4.59	15.93
Cu <sup>II</sup>	45.25	2.91	12.54	49.67	4.55	15.80
Mn <sup>II</sup>	46.07	3.61	12.61	50.48	4.62	16.06
Zn <sup>II</sup>	40.21	3.67	11.26	49.49	4.53	15.74

Crystallization experiments were carried out between L1 and several of the metal nitrate salts over a range of solvents. In each case L1 (20mg) in water was layered below the metal salt (5mg) in a respective solvent and allowed to diffuse slowly. Qualitative analysis of the resulting precipitates is shown in Table 6.

**Table 6 Crystallization attempts for the L1 ICPs**

Solvent (metal)	Metal salt (M(NO <sub>3</sub> ) <sub>2</sub> ·yH <sub>2</sub> O)		
	Co <sup>II</sup>	Cu <sup>II</sup>	Zn <sup>II</sup>
Water	Amorphous	Blue polycrystalline	Amorphous
Acetonitrile	Small pink single crystals	Small blue single crystals	Small single white crystals
Tetrahydrofuran	Amorphous	Amorphous	Amorphous
Methanol	Amorphous	Amorphous	Amorphous

Due to their small size, the single crystals of possible Co and Cu ICPs were sent to the diamond light source scientific facility in south Oxfordshire for X-Ray diffraction analysis.



**Scheme 5 Syntheses of L2 ICP particles from ligand precursor and metal nitrate salts**

**Table 7 Quantities of metal salt reagents for L2 ICP syntheses and the resulting post-reaction precipitate colour.**

M	Quantity	Precipitate colour
Co <sup>II</sup>	119mg, 0.41mmol	Light pink
Cu <sup>II</sup>	95mg, 0.41mmol	Light blue
Mn <sup>II</sup>	95mg, 0.41mmol	Yellow
Zn <sup>II</sup>	122mg, 0.41mmol	White

The syntheses of the L2 ICP particles are outlined in Scheme 5 with reagent quantities as shown in Table 7. As the ligand had quite different solubility properties from the metal salts, room temperature syntheses were carried out in a mixed solvent system. In each case, a dilute solution of L2 (200mg, 0.41mmol) in a chloroform/ethanol mixture (1/1 by volume, 20mL) was slowly added dropwise to a magnetically stirred solution of metal salt (Table 7) in the same mixture (50mL) with immediate precipitate formation in all cases<sup>†</sup>. After complete addition, the reaction mixture was left to stir at room temperature for a further 10min. Additionally, a hot synthesis was performed with copper nitrate for later comparison by AFM. Copper nitrate (95mg, 0.41mmol) in ethanol (30mL) was added dropwise to a magnetically stirred solution of L2 (200mg, 0.41mmol) in ethanol (50mL) at 70°C with the immediate precipitation of a light blue solid observed. This was left stirring for 10min followed by cooling to room temperature. Subsequent isolation steps do not differ from room temperature syntheses.

The resulting suspensions were separated by centrifugation and, if composed of particularly light particles, left to separate under gravity over several days and decanted. The isolated solids were dried under a flow of nitrogen then under vacuum resulting in light particulate solids.

Characterization was performed with AFM and FTIR both of which yielded results for analysis in the discussion section (appendix A7-11).

Crystallization experiments were carried out between L2 and several of the metal nitrate salts over a range of solvents. In each case, L2 (20mg) in chloroform was layered below the metal salt (5mg) in a respective solvent and allowed to diffuse slowly. Qualitative analysis of the resulting precipitates is shown in Table 8.

---

<sup>†</sup> Noting that the rate of precipitation for L2 ICP syntheses was much higher than that of their L1 analogues.

**Table 8 Crystallization attempts for the L2 ICPs.**

Solvent (metal)	Metal salt ( $M(\text{NO}_3)_2 \cdot y\text{H}_2\text{O}$ )			
	$\text{Co}^{\text{II}}$	$\text{Cu}^{\text{II}}$	$\text{Mn}^{\text{II}}$	$\text{Zn}^{\text{II}}$
Ethanol	Amorphous	Amorphous	Amorphous	Ligand crystals
Methanol	Ligand crystals	Amorphous	Amorphous	Amorphous
Acetonitrile	Ligand crystals	Amorphous	Amorphous	Ligand crystals
Dimethylformamide	Ligand crystals	Ligand crystals	Amorphous	Ligand crystals

Upon layering, many of the solvent systems immediately precipitated an amorphous product. This is due to the rate of the L2 reaction being greater than that of its L1 analogues (which were more cooperative in crystallizations).

## Results & Discussion

While the synthesis of many of these compounds appeared to go as planned, characterization is paramount for each reaction in order to gain an insight into these novel compounds. As a result, much of this section is dedicated to the characterization of each compound and the discussion of any interesting findings.

### The ligands

The general reaction for all ligand syntheses was one between a cyclic acid anhydride and a primary amine. While one might expect the resulting ring-open secondary amide to undergo a further condensation reaction with the now carboxylic acid functional group, this only occurred for L2 syntheses. This may be because of the lower (cyclohexene) ring strain in the resulting product as compared with the higher (cyclopentene) ring strain created by the ring closure of L1.

#### Analysis of the novel benzene centred ligands (L1&L3)

$^1\text{H}$  NMR, while supporting the addition of the 1-(3-Aminopropyl) imidazole to the benzene-1,2,4,5-tetracarboxylic dianhydride, is an ambiguous measure of whether the reaction fully ring closed or contained a ring opened carboxylic acid structure (appendix A15). This is due to the molecules symmetry with respect to the locations of hydrogens. Additionally, there appears to be no carboxylic acid or amide peaks; however, the carboxylic acid peak can broaden and not resolve in  $^1\text{H}$  NMR. Amide protons may also have difficulty resolving due to exchange with deuterated solvents (especially  $\text{D}_2\text{O}$ ) but this was done in d-DMSO, making an explanation of its disappearance troublesome. There is a singlet peak at 8.19ppm, a shift that could be the amide proton, but this was concluded to be a residual peak due its presence in a -as confirmed by  $^{13}\text{C}$  DEPT-

decidedly ring closed L3 product which contained only tertiary amides (appendix A15,19-21).

$^{13}\text{C}$  NMR was concluded to be a suitable measure of ring closure. This is due to the symmetry with respect to the carbons being highly affected by ring closure, causing many inequivalent carbons to become equivalent through the introduction of a second mirror plane<sup>‡</sup>. The eleven expected carbon peaks were detected by  $^{13}\text{C}$  NMR, confirming the synthesis of L1 (appendix A16&17).

FTIR produced many peaks from which the presence of a carboxylic acid ( $1644\text{cm}^{-1}$ ), and the ring stretches of imidazole ( $1474$ ,  $1368$ ,  $1345$ , and  $1316\text{cm}^{-1}$ ) were assigned with help from a reference source<sup>11</sup> (appendix A1). These peak assignments will provide a useful insight when comparing them to the metal coordinated compounds.

Elemental analysis results for the L1 syntheses were difficult to work with. The same composition (to within a few parts per thousand) was reproduced for a separate batch of L1 indicating it was not a simple sample wetness issue. Attempts to include solvents, reagents, and possible by-products tended to skew the elemental proportions incorrectly and as such did not prove fruitful in recreating the composition. This, coupled with the MALDI-TOF indicating the existence of many compounds, indicates that a mixture of products may have been produced from the reaction (appendix A13). One major peak in the mass spectrum was at  $432.1\text{Da}$ , the expected weight of the ring closed (L3) compound, which seems to confirm that ring closure is possible without the need for acidification but is not a major reaction product.

Single crystal X-ray diffraction indicated the crystallization of the ring opened species (Figure 5). Hydrogen bonding between the imidazole and carboxylic acid group appears to help hold ligand molecules together within the lattice (Figure 5, bottom). This coordination increases the likeliness of seeing the carboxylic acids involvement in guest metal coordination. Additionally, there appears to be some solvent molecules in the crystal structure, namely acetonitrile and water, both of which were used in ligand crystallization. However, their presence is rather ambiguous due to the low refinement of the structure.

---

<sup>‡</sup> The benzylic and carbonyl carbons being of most interest in this case.

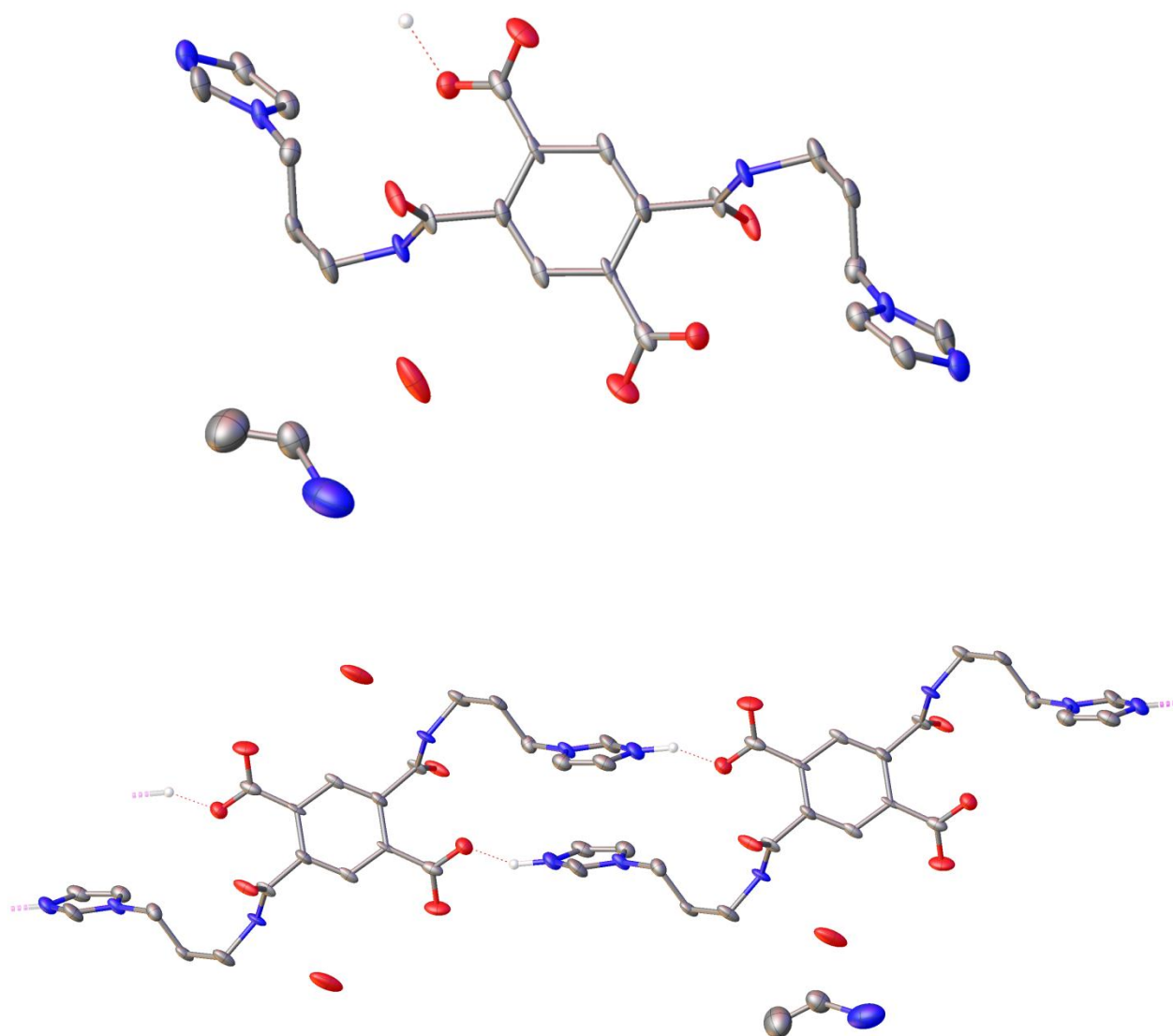


**Figure 5 Top: Partially refined structure of L1. An R-value of 15% was achieved. The proton on the carboxylic group was refined from an unambiguous residual peak and, as can be seen from the grown structure (bottom), appears to create order in the ligands crystal structure.**

The bond angles and lengths around both the carboxylic acid and imidazole are of particular interest and are shown in Figure 6.

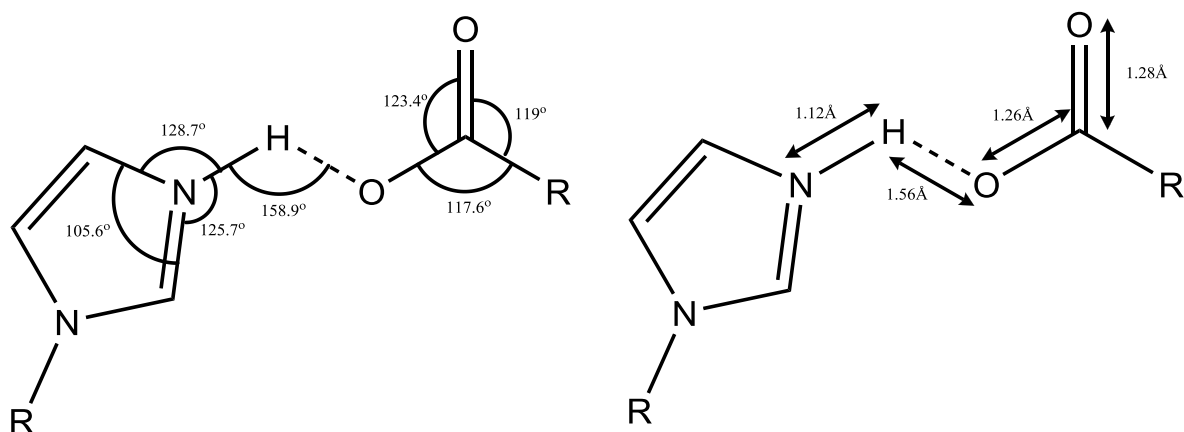


**Figure 6 Left: Bond angles of the hydrogen bridged portion of the molecular structure. Right: Bond lengths of the same structure, noting the similarities between each C-O bond length. Literature examples of carboxylic acids generally have a C-OH and C=O bond lengths of approximately 1.38Å and 1.21Å respectively. Carboxylates have bonds of equivalent length approximately 1.26Å long. Interestingly, the bond length of the non-coordinated (as drawn) oxygen is longer than that of the coordinated one. This may be an aberration of crystal refinement and as such only a fully refined structure would provide a useful insight into the nature of bonding at the carboxylic terminus.**

The length of the hydrogen bond is also interesting. Such a short (<2.8 Å) hydrogen bond is termed a Low-barrier hydrogen bond (LBHB) and could even be classified as a short-strong hydrogen bond (SSHB) as it has a length below 2.29Å. When the distance between donor and acceptor atoms decreases this much the proton is free to move between them (hence low-barrier). LBHBs have been explored between carboxylic acids and 1-methyl imidazole in the literature because of their similarity to the His 57-Asp 102 LBHB<sup>12,13</sup> so, even in the presence of a low-refinement structure, one might expect such a bond to exist for this donor-acceptor pair.

As can be seen from the crystal structure, the proton appears to have migrated onto the imidazole. This may be a consequence of the possible LBHB between the donor and acceptor. The coordinating lone pair on the imidazole is basic as it, unlike on the other available nitrogen, is both orthogonal to the delocalized  $\pi$  bonding system and less sterically hindered. This, compounded by the conjugate base of the donating group being a particularly resonance stabilized carboxylate ion, which can also delocalise some charge into the benzene centre, would make for facile proton migration. This strong hydrogen bonding may explain why L1 was only soluble in water, an extremely polar protic solvent. One might then expect that ring closure would remove this strong interaction increasing the range of cooperative solvents available for further reactions.

As reported in the synthesis section, ring closure of L1 was achieved by reflux in acetic acid. If this was unsuccessful, further attempts with progressively stronger acids could be possible.

$^1\text{H}$  NMR of the ring closed L3 ligand was as ambiguous as its use for L1. The resulting resonances had precisely the same shift and multiplicity as L1 which, while a useful indication that the amine was not somehow addition-eliminated from the molecule, did not appear to indicate if ring closure had occurred. However, as with L1,  $^{13}\text{C}$  provided a revealing measure of ring closure. In addition to the two carbonyl carbons becoming equivalent, ring closure causes two quaternary benzylic carbons to become equivalent. This would cause the originally eleven peaked  $^{13}\text{C}$  spectrum to be composed of nine peaks with the reduction being manifested as the removal of two quaternary carbons.  $^{13}\text{C}$  and  $^{13}\text{C}$  DEPT-135 spectrums indicated this change to be the case, confirming ring closure.

FTIR of L3 was absent of the carboxylic acid peak present in L1 and contained multiple peaks at 1360, 1394, 1442, and 1461 $\text{cm}^{-1}$  as compared with literature values of 1323, 1359, 1486, and 1509 $\text{cm}^{-1}$  for the stretching vibration of unsubstituted imidazoles<sup>11</sup> (appendix A12). Additionally, strong peaks at 1726 and 1775 $\text{cm}^{-1}$ , which is the expected C=O stretching doublet for the structurally similar maleimide occurred, supporting ring closure.

Elemental analysis, as with L1, could not be recreated with any combination of reagent or solvent used as such combinations would skew the proportions of the expected CHN concentrations in the wrong direction.

#### **Analysis of the naphthalene centred ligand (L2)**

$^1\text{H}$  NMR of L2 appeared to support the formation of the ligand, noting that two imidazole peaks (at 7.01ppm) merged into a multiplet (appendix A18). Unlike for L1 and L3 syntheses,  $^{13}\text{C}$  NMR is not a necessity here to confirm ring closure as the naphthalene centre contains four protons that would be affected by a change of molecular symmetry (i.e. split if the product was ring-opened).

FTIR peaks of interest for L2 included the carboxylate peak at 1654 $\text{cm}^{-1}$  and the imidazole peaks at 1345, 1375, 1456, and 1509 $\text{cm}^{-1}$  (appendix A18). The imidazole shifts differed somewhat from the unsubstituted imidazole literature shifts<sup>11</sup> but this is to be expected of an alkyl substituted analogue.

Refined single-crystal X-ray diffraction models for L2 were provided by V. J. Richards, a colleague who originally started work on the naphthalene centred ligand and provided the synthetic method used in this study (Figure 7).

Elemental analysis and ES-MS of L2 confirmed the synthesis of L2 with a mass peak of 482.17Da and a less than 0.2% deviation between the expected and found elemental compositions (appendix A14).

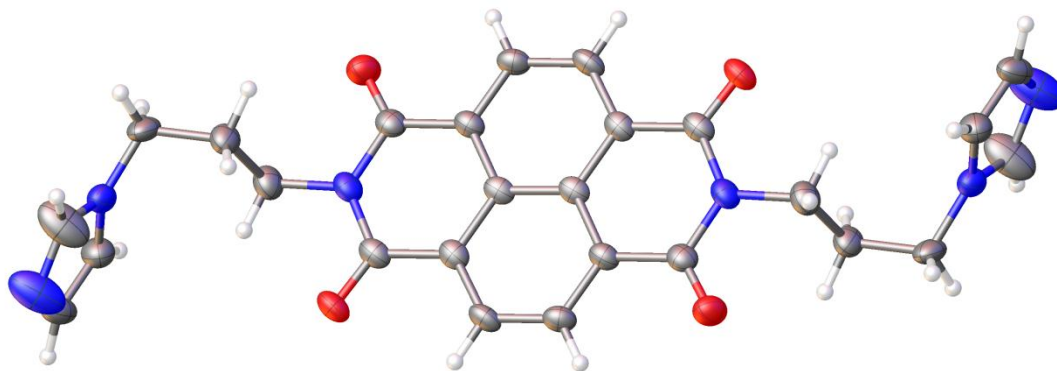


**Figure 7 Single-crystal x-ray diffraction structure of L2. An R-value of 10% was achieved. Here, it appears that ring closure occurs without the need for acidification. As a point of interest, the C=O bond length is 1.20Å, a typical C=O bond length. Source: V. J. Richards.**

## ICPs

As reported in the synthesis section, fabrication of the ICP particles was practically very simple. Each specimen was made by the reaction of a ligand (L1 or L2) with a metal nitrate salt to form a, presumably 2+ charged, metal coordination compound. In addition to the somewhat sterically hindered backbone of the ligand (i.e. the benzene or naphthalene centre), the spatial remoteness of the imidazole electron donors increase the likeliness of them to act as bridges rather than chelating donors. For this reason, a polymeric metal-organic compound is expected to form. These compounds can be formed as micro- and nanoscale particles rather than as macroscopic materials.

The coordination mechanism, which acts as the basis for polymeric growth, leaves uncoordinated imidazoles inside but, more importantly, at the surface of the particle. This allows for further growth of the particle provided there is metal cation and ligand present in solution. Because of this, the condition and solvent system of the reaction may have a large impact on the growth of the particles. For these experiments, all reactions are done at room temperature with vigorous stirring to encourage controlled particle growth. However, this is conjecture, systematic studies with respect to reaction conditions, solvent, etc in the field of ICPs remains sparse so deciding on the ideal practical variables for these reactions was based on a combination of similar previous works and qualitative approaches<sup>3,4</sup>.

One might expect that these nanoscale particles may exhibit largely different properties from their macroscopic analogues. Unlike single-component nanoparticles (gold, copper, etc) the nanoscale spatial dimensions of these particles are less likely to cause a

dramatic change in the electronic properties of the substances<sup>§</sup> which is typically a source of interesting differences between nano- and macroscale materials. That is not to say that these particles will not observe special properties as a result their size, but it is more likely to manifest as a high surface activity rather than, for example, a dramatically different colour.

Most reactions produced a precipitate which, upon isolation, had the colours expected of their metal occupancy (pink cobalt, blue copper, white zinc, etc) manganese (II) appeared to take longer for L1 syntheses and produce an unexpectedly yellow compound in L2 syntheses. The increased duration for precipitate formation in L1 syntheses could in fact be precipitation of the starting ligand which needs to be carefully considered when looking at the FTIR and elemental compositions of the product. The yellow product from L2 manganese (II) syntheses could be precipitating ligand, but both the dissolved metal salt and ligand pre-reaction were in the same solvent mixture at a temperature well below its boiling point (at which temperature the chloroform/ethanol would proportionally increase in ethanol concentration aiding precipitation of the ligand); additionally, the yellow precipitate immediately begun to precipitate out upon addition of a dilute solution of the metal salt at much the same rate as the other L2 ICP syntheses.

What differs from the literature examples is that the ICPs in the study spontaneously precipitated out of solution, this makes controlling their size troublesome when compared with the more popular method of using a second solvent to arrest the polymerisation and precipitate the compound.

FTIR is ideal for situations where the bonding structure of a compound can be compared pre- and post-reaction. In this case, the interest is in any shifts to the imidazole and carboxylic acid absorptions. The peaks of interest were identified as  $1644\text{cm}^{-1}$  for the carboxylic acid, 1474, 1368, 1345, and  $1316\text{cm}^{-1}$  for the imidazole in uncoordinated L1 (appendix A1). Similar peaks were found in the coordinated compound as shown in Table 9.

---

<sup>§</sup> This is more likely in single component metallic systems due to 'particle in a box' style effects which work best for the delocalized electronic systems that metallic compounds tend to exhibit.

**Table 9 Vibrational peaks of interest from L1 and coordinated L1 reaction products as KBr pellets (cm<sup>-1</sup>). Assignments were made with aid from a literature source for unsubstituted imidazole in D<sub>2</sub>O solution<sup>11</sup>. Ambiguous assignments are tinted. Appendix references: Co<sup>II</sup>, A2; Cu<sup>II</sup>, A3; Mn<sup>II</sup>, A4; Zn<sup>II</sup>, A5.**

Assignment	Literature value XXX(unsubstituted imidazole)	Uncoordinated L1	Metal coordinated			
			Co <sup>II</sup>	Cu <sup>II</sup>	Mn <sup>II</sup>	Zn <sup>II</sup>
C=O str.	N/A	1644	1621	1634	1622	1632
Ring str.	1509	1474	1465	1490	1465	1489
Ring str.	1486	1368	1404	1404	1403	1401
Ring str.	1359	1345	1363	1384	1362	1384
Ring str.	1323	1316	1337	1342	1337	1340

Peaks assigned in the uncoordinated L1 were seen in the coordinated analogues at shifted frequencies. As the reference source suggests, the level of shift is dependent upon the strength of the metal nitrogen bond. An extremity of these shifts being the formation of an imidazolium ion by protonation. Higher imidazole ring stretches are indicative of stronger metal-nitrogen bonding. The highlighted Co<sup>II</sup> and Mn<sup>II</sup> stretches appear to break this pattern, decreasing relative to the starting material. This is difficult to explain as it would implicate that there was somehow more electron density on the nitrogen lone pair relative to the starting material. All the other stretches change by upwards of 10cm<sup>-1</sup> indicating electron redistribution resulting from inductive electron withdrawal operating at the pyridine region. It does appear that the ligand did coordinate to the manganese (II) as shown by a change in both the C=O and imidazole ring stretches.

What is interesting is that the C=O stretch was shifted downwards by coordination. This is indicative of a weakening of the C=O bond (or rather, a lowering of its bond order) which implies the involvement of the carboxylic acid in coordination. This is very likely as the carboxylic acid, which is susceptible to deprotonation, can readily change into a carboxylate ligand.

FTIR of L2 shown peaks of interest at 1654cm<sup>-1</sup> for the C=O stretch, 1509, 1456, 1375, and 1345cm<sup>-1</sup> for the imidazole stretches (appendix A6). Similar peaks found in the coordinated compounds are shown in Table 10.

**Table 10 Vibrational peaks of interest from L2 and coordinated L2 reaction products as KBr pellets ( $\text{cm}^{-1}$ ). Assignments were made with aid from a literature source for unsubstituted imidazole in  $\text{D}_2\text{O}$  solution<sup>11</sup>. Appendix references:  $\text{Co}^{\text{II}}$ , A7;  $\text{Cu}^{\text{II}}$ , A8;  $\text{Mn}^{\text{II}}$ , A10;  $\text{Zn}^{\text{II}}$ , A11.**

Assignment	Literature value XXX(unsubstituted imidazole)	Uncoordinated L2	Metal Coordinated			
			$\text{Co}^{\text{II}}$	$\text{Cu}^{\text{II}}$	$\text{Mn}^{\text{II}}$	$\text{Zn}^{\text{II}}$
C=O str.	N/A	1654	1663	1662	1654	1667
Ring str.	1509	1509	1522	1523	1519	1528
Ring str.	1486	1456	1456	1456	1455	1455
Ring str.	1359	1375	1384	1384	1384	1384
Ring str.	1323	1345	1342	1341	1341	1342

There is a smaller change in the C=O shift between coordinated and uncoordinated species. This is expected for the, presumably ring closed, tertiary amide carbonyl would not coordinate as readily to metals as a carboxylic acid or carboxylate group. However, a shift of approximately  $10\text{cm}^{-1}$  still occurs for all but manganese (II). This amount of shift could still be indicative of the carbonyl playing a key role in metal coordination.

The changes in imidazole stretches appear to be smaller relative to L1 syntheses. This is unexpected as the pyridine-like nitrogen on the imidazole is the most probable coordination location available on the ligand. Additionally, there appear to be little differences in imidazole stretches between each metal with the only differences larger than  $1\text{cm}^{-1}$  occurring for the highest imidazole stretches ( $1522$ ,  $1523$ ,  $1519$ , and  $1528\text{cm}^{-1}$ ). These findings would appear imply that the metal ligand interaction is comparatively weaker than that offered by L1. The rate of precipitation for L2 syntheses was noticeably faster than for L1 which may lead one to believe that the kinetic and thermodynamic boundaries to formation are favourable. While the FTIR data supports the notion that the bonding interactions (and therefore exothermicity) produced by the L2 reactions are weaker, the stark differences in reaction kinetics may be dictated by the solvent system employed, which is different between the two syntheses. However, as previously mentioned, there is a lack of systematic studies into the effect of solvent systems on the fabrication of ICPs.

Concerns about whether the coordination to manganese (II) was successful are somewhat resolved by the FTIR data, many of the imidazole L2 peaks have shifted much post-addition but there appears to be no shift in the C=O stretch.

Of the crystals produced by the layering experiments zinc coordinated crystals appeared successfully yielded a workable X-Ray diffraction pattern (Figure 8).

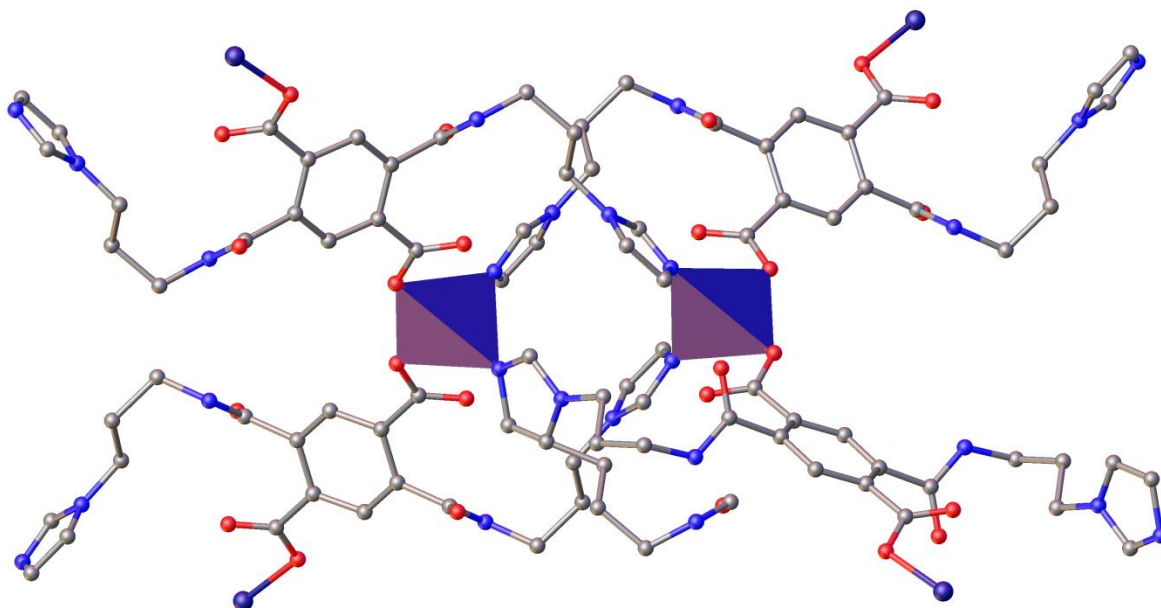


**Figure 8** Partially refined structure of the L1-coordinated zinc MOF. An R-value of 15% was achieved. Here, the zinc cations are represented as blue tetrahedral shapes for clarity. In addition to the predicted imidazole donor, the carboxylic acid/carboxylate coordinates to the metal centre. Because of this, a single ligand may be in fact coordinated to four separate metal centres. This encourages polymeric growth of a metal-ligand coordinated structure. Due to the lack of refinement, it is difficult to say exactly where the carboxylic acids proton may be. This may be significant when considering the overall charge of the complex as such an easily ionized proton could help charge-stabilize the complex as a whole rather than requiring the presence of  $\text{NO}_3^-$  anions somewhere within its structure.

As predicted from the FTIR data, the carboxylic group is involved in coordination to the metal. Due to the lack of refinement in the crystal structure, it is difficult to say exactly where the carboxylic acids proton may be. This may be significant when considering the charge stabilization of the 2+ charged complex. One might postulate that the proton migrated fully onto the nitrate counter-anions present in the reagent salt. This may be the case because no residual peaks in the crystal structure appeared to match the expected trigonal-planar geometry of a nitrate anion. Its absence would be expected if it was completely vacant from the structure altogether due to proton migration to create nitric acid; however, the low pKa of nitric acid would mean proton migration only be thermodynamically favourable if the creation of a metal-coordinating carboxylate functionality would indeed be energetically favourable overall. Considering the overall structure of this MOF, this may be the case. But such postulations are conjecture when reminded of the overall poor refinement of this crystal structure.

Bond length and angle measurements were also taken for this structure in order to determine what the driving force for coordination was (Figure 9). As can be seen, the

bond length of the carboxylate and imidazole donors does not vary dramatically. Likewise, the C-O and C=O bond lengths of the carboxylic acid group, which differ by 0.4 Å, do not appear to support the formation of a carboxylate.

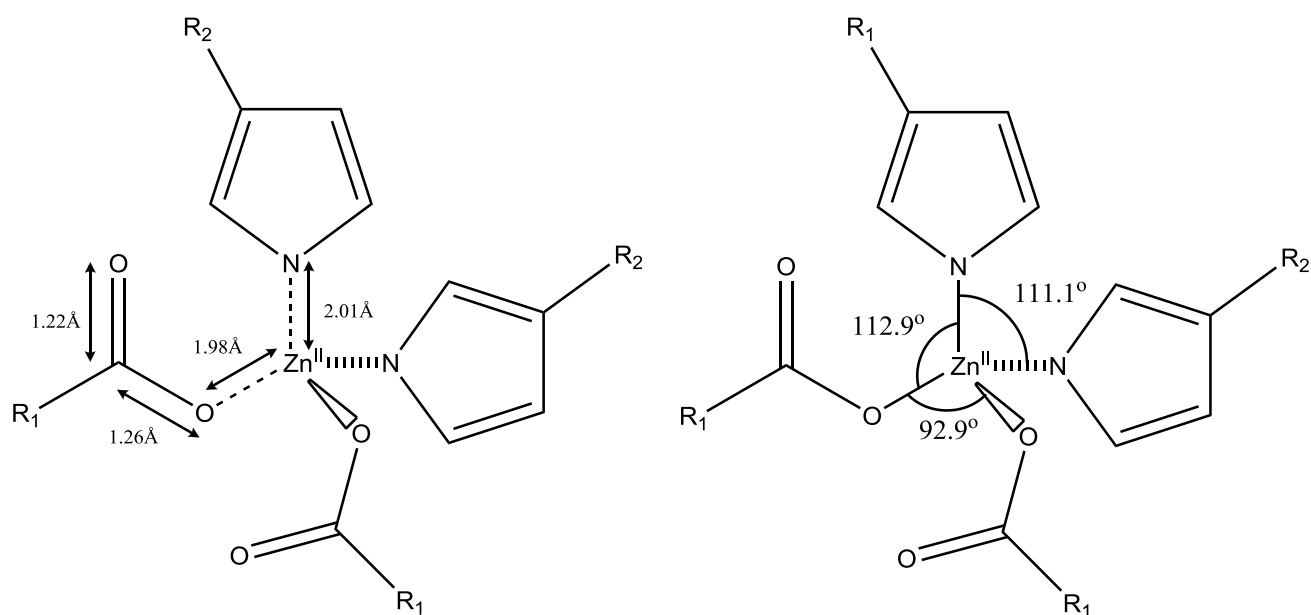


**Figure 9 Bond lengths and angles of L1's coordination to the zinc centre derived from single-crystal X-Ray diffraction. Bond lengths of 2.00Å for the imidazole and 1.98Å for the carboxylic acid group closely match similar bond lengths found in the literature (PROTEIN).**

The recorded bond angles are also of great interest. O-Zn-O appears to be much smaller than the O-Zn-N and N-Zn-N angles. One might argue that the immediate steric bulk of an imidazole ligand outweighs the two-atom displaced bulk of the benzene centre. While this would explain why the imidazole donors appear to be "pushing" the carboxylic acid donors together, a 20° difference in bond angle seems rather dramatic. Figure 10 shows the overall structure of two coordinated metals.

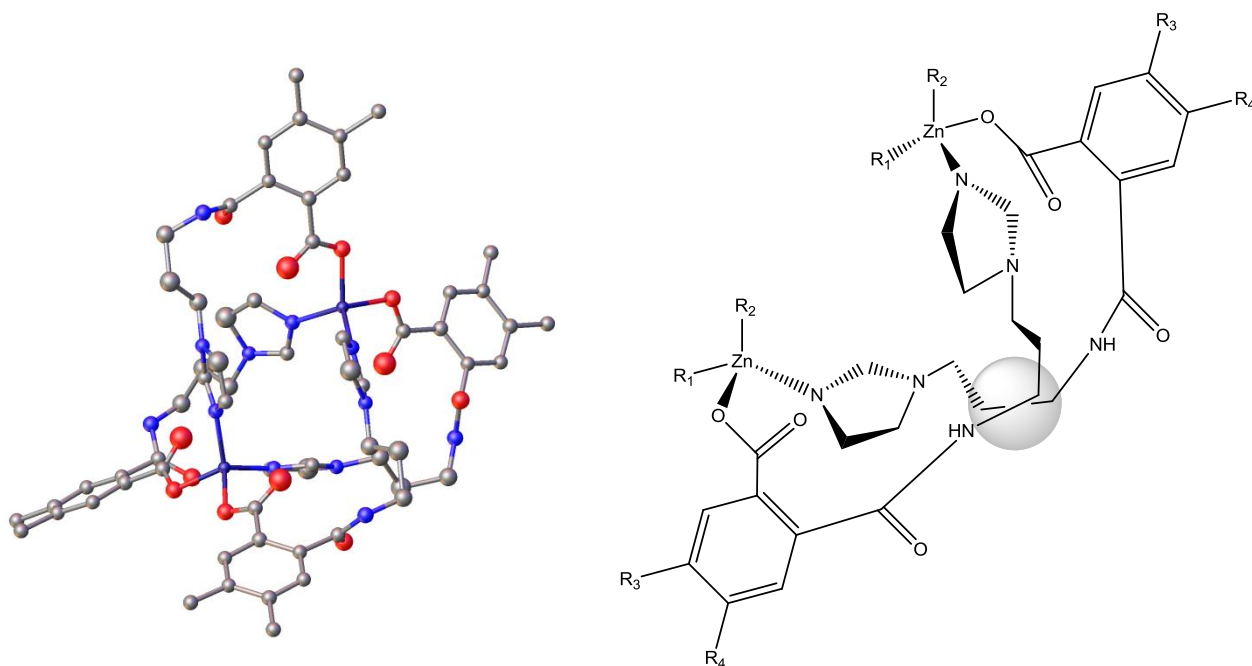
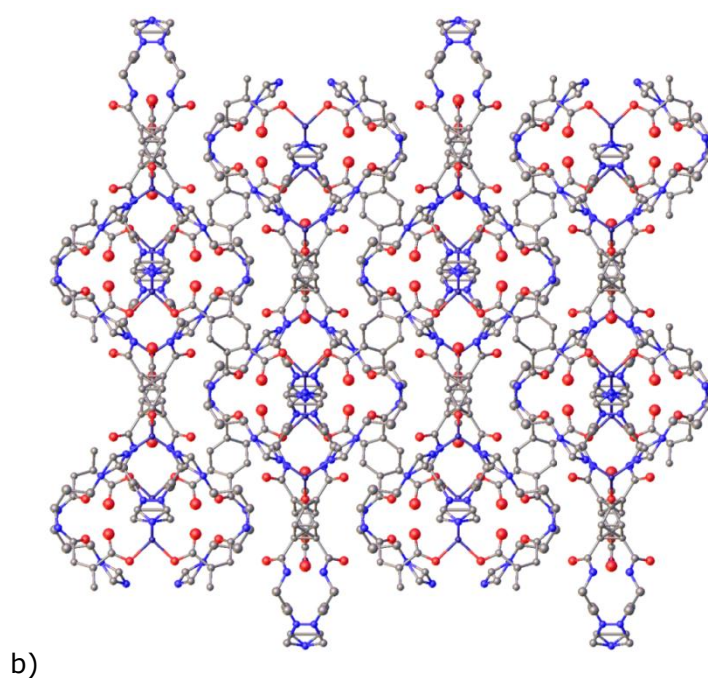
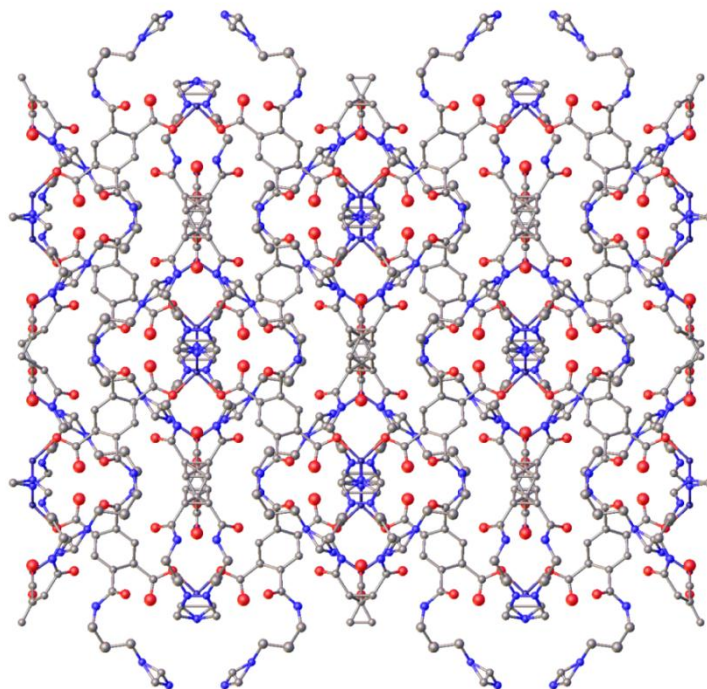


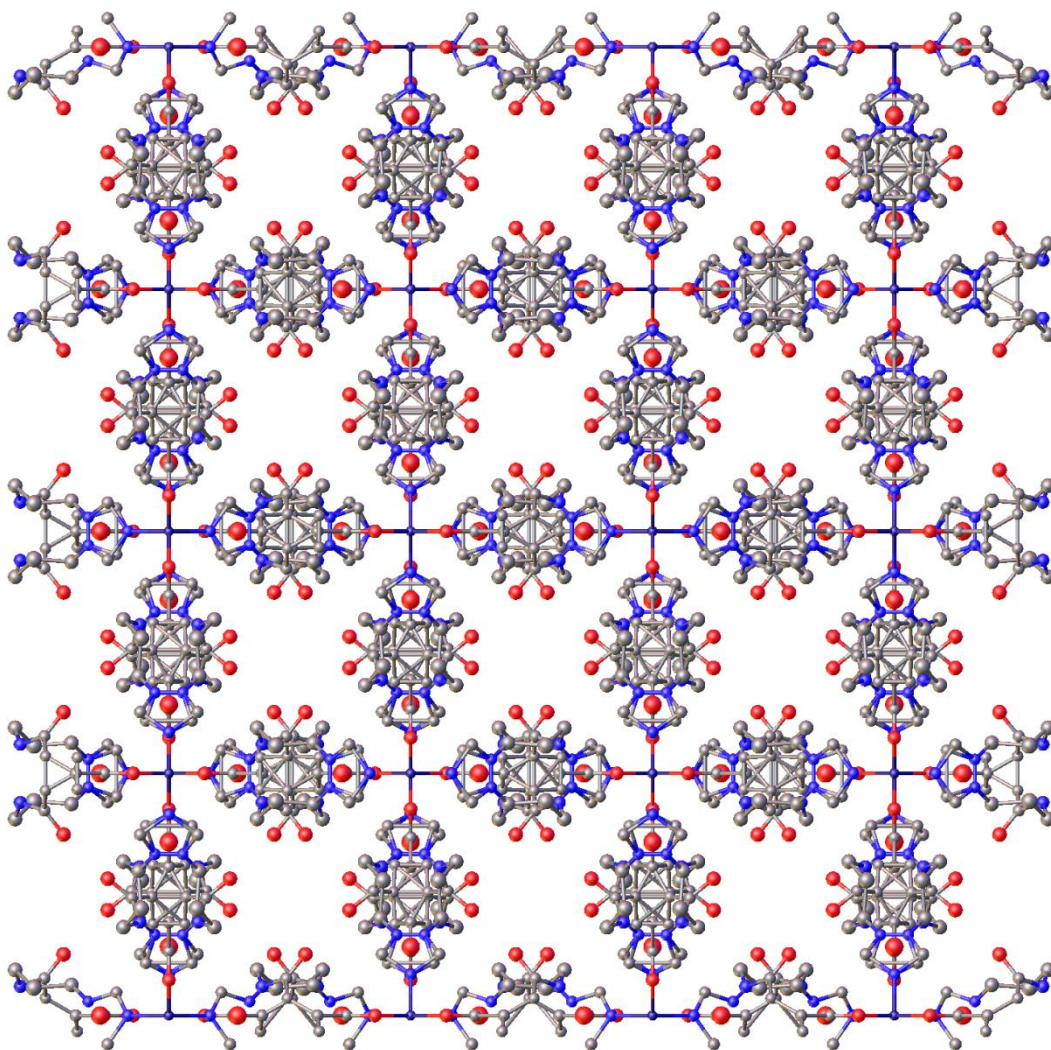
**Figure 10** Left: Simplified view of the bonding structure taken by the complex as a whole. Right: schematic diagram of one carboxyl-imidazole binding, the point of crossover highlighted as a grey circle. Here, it can be seen that the one ligand will cross over another as it coordinates to the next adjacent metal. The bonding structure taken by the complex is extremely cooperative in the sense that each metal is coordinated to four different ligands which, in turn, are weaved between other metal centres to create a supramolecular structure overall as opposed to discrete motifs. This ordered macrocyclic structure may relieve the conformational strain required for a long chain to coordinate to a nearby metal by pushing the two, less sterically strained, carboxylic acid ligands to within closer than normal proximity.

The bond angle observations appear to be a result of the well-ordered structure of the complex. The ligand must go into a particular conformation in order to meet the geometrical requirements of coordinating to the second metal. These requirements could be met by conformational rearrangement (i.e. the molecule contracting using eclipsed and gauche conformations as opposed to the preferred anti conformations) but it appears that some of the strain may be released by pushing the carboxylic acid coordinating points together, allowing the imidazole-end of the ligand to extend slightly more without using unfavourable conformations the alkyl chain.

A major point of interest for MOFs is their potential ability to store guest species. The well-ordered supramolecular structure of a MOF, which may also contain coordination groups and the like, offers an enthalpically favourable site in which a guest molecule may reside. This is useful in the context of gas storage because the site increases the Gibbs free energy of vaporisation for a species at a particular temperature or pressure allowing the storage of a large amount of gas at lower volumes with a lower pressure requirement. A major scientific hurdle in the production of hydrogen fuelled automobiles remains its storage. High pressure hydrogen cylinders, which are a working method of

hydrogen storage, are cumbersome and dangerous. ICP based storage solutions allow hydrogen to be stored more reasonably, which is why they are currently are a field of major scientific interest. The cavity structure of the L1 Zn MOF is shown in Figure 11.





c)

**Figure 11 Grown crystal structures of the L1 coordinated Zn MOF. The structure had an R-value of 15%. The confusing appearance of the central ligand positions is, for the most part, a manifestation of the rotational disorder that occurred in the benzene and alkyl backbone of the ligand that was not properly removed from the unit cell. a) Crystallographic a-axis. b) Crystallographic b-axis. c) Crystallographic c-axis. The c-axis appears to have a well ordered cavity structure with carbonyl inward-pointing carbonyl groups**

While the crystallographic a- and b-axis did not appear to have a very ordered pattern, the c-axis was a much more obvious as a host axis for guest molecules. The cavity has a  $5.46\text{\AA}$  by  $5.46\text{\AA}$  cross section (from top carbonyl to top carbonyl) which may be a suitable size for certain guests although further experimentation would be required to confirm the usefulness of this MOFs cavity.

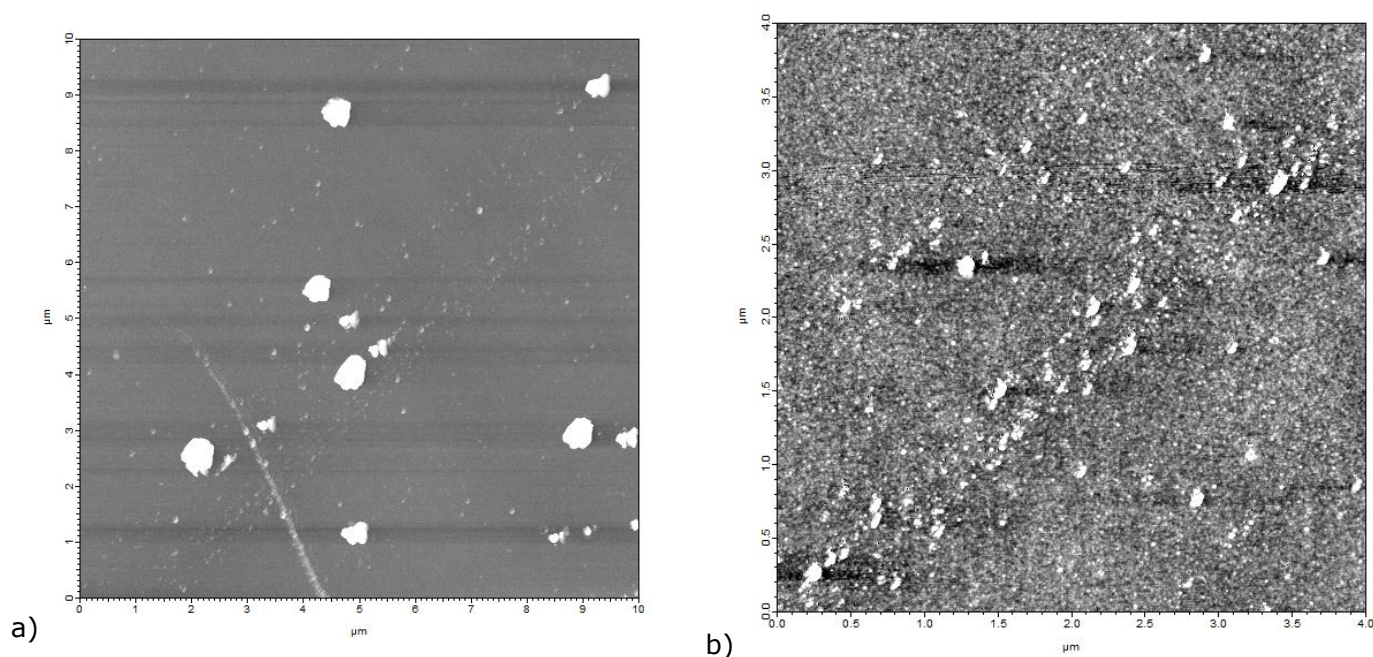
Elemental composition was only measured for L1 ICP syntheses due to time constraints. Much like the issues encountered for the reproducing the elemental composition of L1, there does not appear to be any integer amount of solvents or reagents that reproduces the elemental composition found. Attempts to use combine the MALDI-TOF and elemental composition data to reproduce the proportion change observed post-

metalation (Equation 1) did not appear to suggest that any of the other MALDI peaks may have been responsible for the precipitated compound.

**Equation 1 Used to scale all L1 MALDI peaks into a metal coordinated composition; unfortunately, no peaks scaled the L1 compositions to match those found for the L1 MOFs.**

$$\text{Rescaled composition(\%)} = \text{Original composition(\%)} * \left( \frac{\text{MALDI peak}}{\text{MALDI peak} + x\text{Metal}} \right)$$

Of the characterization techniques discussed, all have looked at the chemical and molecular composition of the ICPs. AFM scans of the ICPs can provide a valuable insight into the particle growth mechanism and general spatial dimensions of the particles made. For the scans, ICP samples were suspended in ethanol and drip coated onto a clean {100} boron-doped silicon surface\*\*. This oxygen-terminated surface was chosen purely because of its atomic evenness which would serve as an ideal backdrop to the MOF particles. Scans for the L1 ICPs are shown in Figure 12.



---

\*\* Cleaned by sonication in several solvents to ensure no contaminants were present on the surface: acetone, methanol, and iso-propyl alcohol.

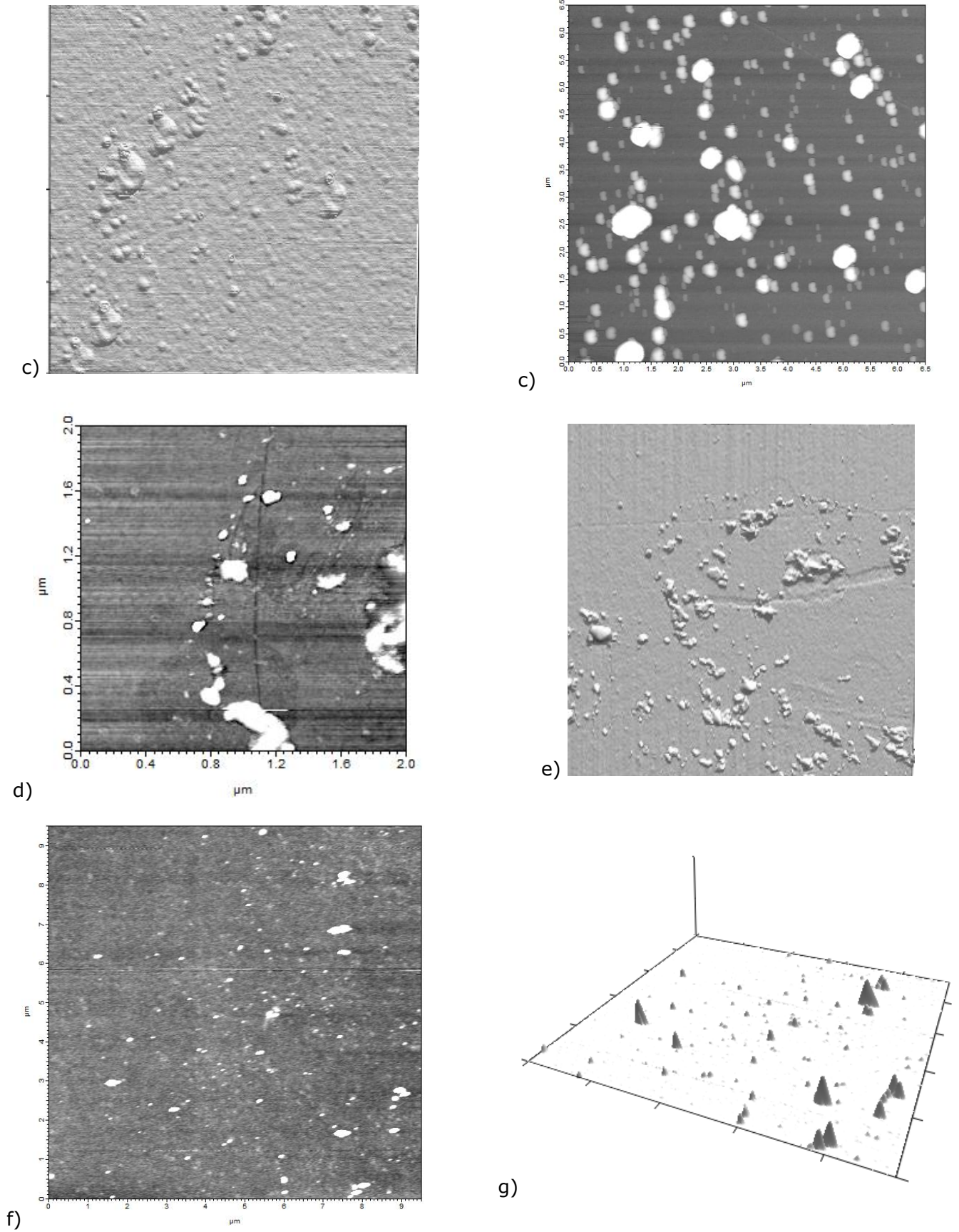


**Figure 12** AFM scans of drop coated L1 ICPs taken with the MFP-3D standalone AFM. a)  $\text{Co}^{\text{II}}$ , b)  $\text{Co}^{\text{II}}$  (zoomed), c)  $\text{Co}^{\text{II}}$  (shaded), d)  $\text{Cu}^{\text{II}}$ , e)  $\text{Mn}^{\text{II}}$ ,  $\text{Zn}^{\text{II}}$ , and  $\text{Zn}^{\text{II}}$  (3d)

The shapes of all particles appear to be close to spherical. From the bond lengths shown in the x-ray derived structures and the relative rate of the reaction at room temperature, particle growth appears to be kinetic in nature. That is to say that slow, equilibrated, and thermodynamic growth would most probably lead to a much more geometrically sound particle (well-rounded spheres, octahedrons, etc).

Particle sizes were measured for the scans and plotted onto a histogram. Particle size was taken as 50% of the cumulative frequency. Sizes of 45, 7, 5, and 3nm were found for cobalt, copper, manganese, and zinc respectively. There does not appear to be any correlation between the metal centre and the resulting particle size but would be expected of a precipitation mechanism that may be highly affected by temperature and solvent than reaction thermodynamics.

Scans for the L2 ICPs are shown in Figure 13. Due to practical limitations, only scans of the copper and zinc species were taken. The uneven shapes of the particles may be as a result of the even faster rate of precipitation for L2 syntheses which would lead to less equilibrated structures than the L1 analogues. The copper hot synthesis was performed before the room-temperature solvating mixture (chloroform/ethanol) was found to be a working solvent system. Because of this, it is done in ethanol at 70°C (lower temperatures would result in reagent precipitation).

Particle sizes for the three scanned L2 ICPs were taken in the same manner as L1. Sizes of 25, 4, and 5nm for Cu<sup>II</sup>(hot), Cu<sup>II</sup>(room temp), and Zn<sup>II</sup> respectively were found. While the sizes for the room temperature copper (II) synthesis and zinc (II) closely match those found for L1, the particle size for the hot synthesis is significantly larger than both (25nm). This is surprising as one would expect an increased rate of reaction, and therefore precipitation, would lead to smaller particles. This synthesis was carried out in a more polar solvent system which, when considering that the resulting particles would presumably contain a high percentage of organic ligand on their surface, would encourage surface energy minimization by particle growth. However, because this reaction was also done in a different solvent system it is unwise to extrapolate any quantitative models for growth from this finding.

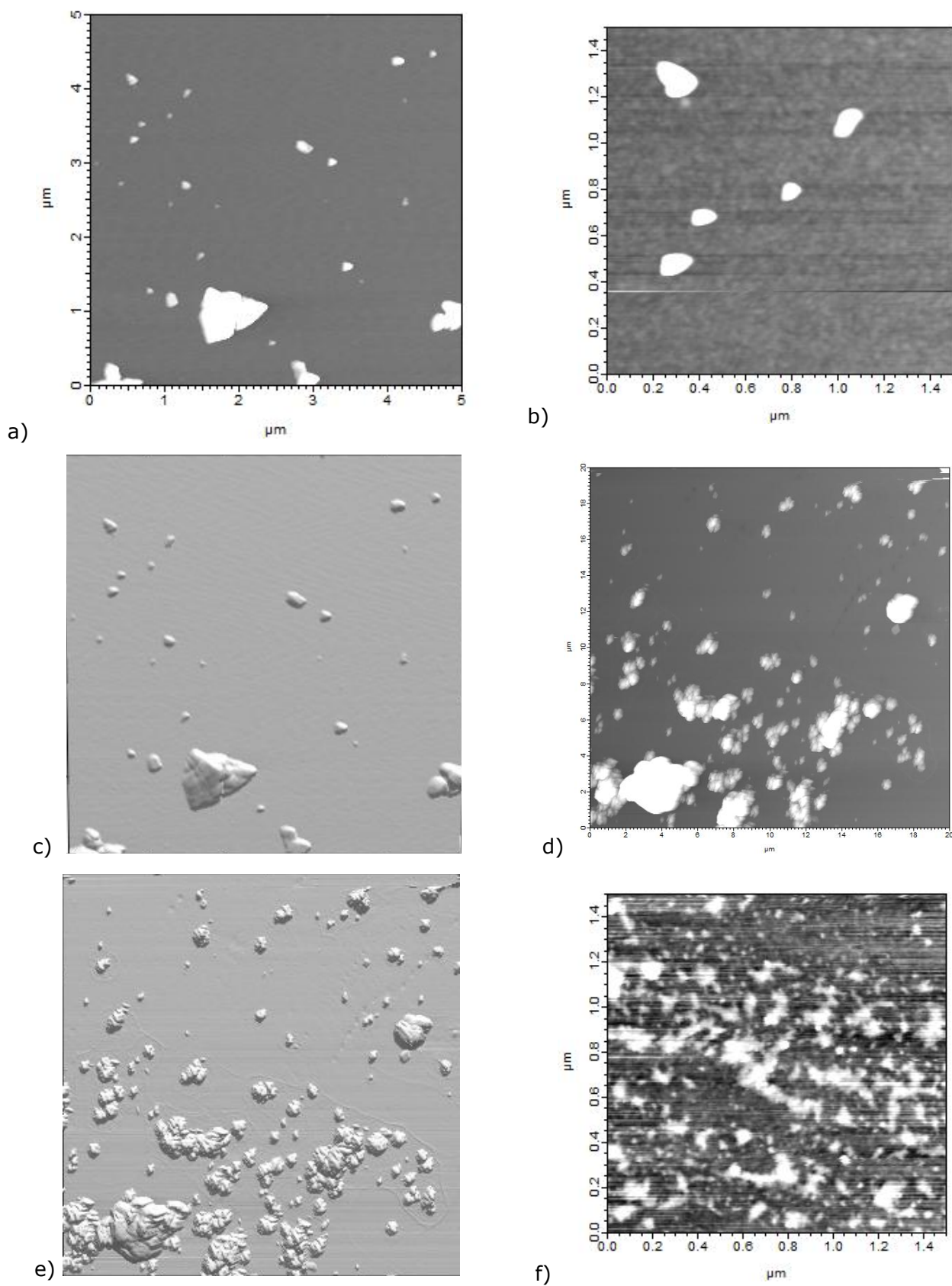


**Figure 13** AFM scans of the drop coated L2 ICPs taken with the MFP-3d standalone AFM. a) Cu<sup>II</sup> (hot synthesis), b) Cu<sup>II</sup> (zoomed, hot synth.), c) Cu<sup>II</sup> (shaded), d) Cu<sup>II</sup> (room temp), e) Cu<sup>II</sup> (shaded), and f) Zn<sup>II</sup>.

## Conclusion

Synthesis of a new multidentate ligand was characterized and shown, upon metalation, to take a crystallographically well-ordered structure that appears to have an axis of porosity about it. However, further investigations are necessary to confirm the usefulness of such porosity. What is interesting is how such an ordered structure forms from an, alkyl chain containing, multidentate ligand with the necessary flexibility to form a less ordered structure. Literature examples appear to use conformationally restricted multidentate ligands; for example, the 2,2-bipyridine backboned ligands used in grid and helicate fabrication, as a method of fabricating large frameworks. An interesting venture would be to see how this idealized, low temperature, and slowly grown structure is applicable to the amorphous ICP particles made in these syntheses.

Nevertheless, the high surface area offered by these nanoscale particles could outweigh the disadvantages brought on by their lack of crystallinity. Literature sources on amorphous ICP particles appear to be optimistic about their applicability in fields such as hydrogen storage, and catalysis. What is remarkable is the apparent stability of these species, which shown no visible sensitivities to changes in temperature and could be suspended in a range of solvents without any signs of dissolution<sup>††</sup>.

Solvent choice appears to be paramount when synthesising this class of materials. Literature sources have reported that solvent choice can be the deciding factor between a highly crystalline or highly amorphous product. The size of the resultant particles may also be heavily controlled by the choice of solvent. The particles precipitated spontaneously from the reaction mixture making control of the particle size by varying the addition rate of the precipitating solvent impossible. This study was quite restricted in this context because both of the ligands were only soluble in a small subset of polar solvents. As more research is published in this area a reliable model for solvent choice may come together.

There are many possible adaptations for set of ligands studied here such as a longer alkyl chain, a perylene backbone, or an enhanced nitrogen donor to name a few. What is impressive is that this class of particles have been reported to offer an interesting degree of chemical flexibility in other studies<sup>2-6,8,9,14</sup>. Processes such as metal exchange and ligand tuning have been reported making this research field potentially quite expansive and adaptable in its applications.

---

<sup>††</sup> Keeping in mind that all solubility tests would test dissolution at any temperature up to the boiling point of the solvent.

# References

- (1) Champness, N. R. *Angew. Chem.-Int. Edit.* 2009, 48, 2274.
- (2) Imaz, I.; Hernando, J.; Ruiz-Molina, D.; Maspoch, D. *Angew. Chem.-Int. Edit.* 2009, 48, 2325.
- (3) James, S. L. *Chem. Soc. Rev.* 2003, 32, 276.
- (4) Spokoyny, A. M.; Kim, D.; Sumrein, A.; Mirkin, C. A. *Chem. Soc. Rev.* 2009, 38, 1218.
- (5) Imaz, I.; Maspoch, D.; Rodriguez-Blanco, C.; Perez-Falcon, J. M.; Campo, J.; Ruiz-Molina, D. *Angew. Chem.-Int. Edit.* 2008, 47, 1857.
- (6) Jeon, Y. M.; Armatas, G. S.; Heo, J.; Kanatzidis, M. G.; Mirkin, C. A. *Adv. Mater.* 2008, 20, 2105.
- (7) Jeon, Y. M.; Heo, J.; Mirkin, C. A. *J. Am. Chem. Soc.* 2007, 129, 7480.
- (8) Jung, S.; Oh, M. *Angew. Chem.-Int. Edit.* 2008, 47, 2049.
- (9) Oh, M.; Mirkin, C. A. *Nature* 2005, 438, 651.
- (10) Tansil, N. C.; Xie, H.; Xie, F.; Gao, Z. Q. *Anal. Chem.* 2005, 77, 126.
- (11) Carlson, R. H.; Brown, T. L. *Inorg. Chem.* 1966, 5, 268.
- (12) Cassidy, C. S.; Reinhardt, L. A.; Cleland, W. W.; Frey, P. A. *J. Chem. Soc.-Perkin Trans. 2* 1999, 635.
- (13) Tobin, J. B.; Whitt, S. A.; Cassidy, C. S.; Frey, P. A. *Biochemistry* 1995, 34, 6919.
- (14) Oh, M.; Mirkin, C. A. *Angew. Chem.-Int. Edit.* 2006, 45, 5492.

# Appendix

Appendix figures are labelled A1-21 with the following content:

1. **A1-12**: FTIR data
  - a. **A1**: L1
  - b. **A2-5**: L1 ICPs
  - c. **A6**: L2
  - d. **A7-11**: L2 ICPs
  - e. **A12**: L3
2. **A13**: MALDI-TOF of L1
3. **A14**: ES-MS of L2
4. **A15-21** NMR data
  - a. **A15-17**: L1
  - b. **A18**: L2
  - c. **A19-21**: L3